Calix[4,6,8]arenesulfonates Functionalized Reduced Graphene Oxide with High Supramolecular Recognition Capability: Fabrication and Application for Enhanced Host−Guest Electrochemical Recognition

Jun Zhou,[†,‡] Ming Chen,[†] and Guowang Diao*,[†]

[†]College of Chemistry and Chemical Engineering, Yangzhou University, Yangzhou 225002, Jiangsu, People's Republic of China
[‡]Nantong Vocational College, Nantong 226001, Jiangsu, People's Republic of China

Ⓢ *Supporting Information*

ABSTRACT: Reduced graphene oxide (rGO) modified with three kinds of water-soluble p-sulfonated calix[4,6,8]arene sodium (SCn: SC4, SC6, SC8) were successfully prepared by using a simple wet chemical strategy. Three obtained SCn-rGO nanocomposites were characterized by Fourier transform infrared spectroscopy, Ultraviolet−visible spectroscopy, static contact angle measurement, thermogravimetric analysis, scanning electron microscope and electrochemical impedance spectroscopy, which confirmed that different amount of SCn molecules had been effectively loaded onto the surface of rGO, and the water-dispersity and stability of SCn-rGO increased with the increase of the value of n in SCn ($n = 4, 6, 8$). More significantly, cyclic voltammetry measurement showed that the SCn-rGO could exhibit high supramolecular recognition and enrichment capability and consequently displayed excellent electrochemical response toward four probe molecules (biological and organic dye molecules). Especially, SC8-rGO exhibited an excellent electrochemical performance for dopamine with high current densities of 73.04 mA mM^{-1} L cm^{-2}, broad linear range (1×10^{-8} to 2.1×10^{-5} M) and very low detection limit (8×10^{-9} M) at a signal-to-noise ratio of 3.

KEYWORDS: *reduced graphene oxide, calix[4,6,8]arenesulfonates, supramolecular self-assembly, graphene nanocomposites, host−guest recognition, electrochemical detection*
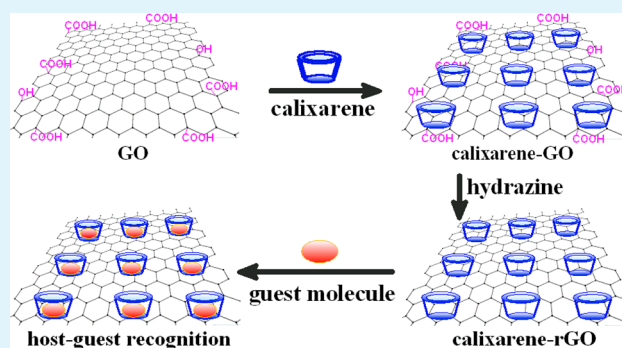
1. INTRODUCTION

In recent years, graphene, as a two-dimensional material (2D), has attracted considerable attention on the horizon of material science because of remarkable and unique properties, such as excellent mechanical properties,[1] extremely high specific surface area,[2] and fascinating electronic transfer at room temperature.[3] These outstanding properties support graphene as an ideal building blocks in nanocomposites and also holding great promise for potential applications in many scientific fields such as catalysis,[4−6] sensors,[7,8] energy storages,[9,10] electronics,[11,12] and photonics.[13]

The reduced graphene oxide (rGO), obtained by reduction of graphene oxide (GO), although its conductivity is comparatively lower than that of the mechanically cleaved graphene, is nevertheless versatile materials. However, rGO is hydrophobic and easily forms agglomerates irreversibly through strong $\pi-\pi$ stacking interaction in an aqueous solution,[14] which extremely restricts its application in many field in aqueous solution. Therefore, the functionalization of rGO has been considered to be important for improving their solubility. Up to now, various types of molecules have been attempted to disperse rGO to avoid rGO aggregation in water, such as covalent or noncovalent attachment of poly (3,4-ethyldiox-

ythiophene),[15] 1-pyrenebutyrate,[16] Methylene Green,[17] Py-ssDNA,[18] DNA,[19] and poly(sodium 4-styrenesulfonate)[20] onto the rGO surface. Nevertheless, in most cases, dispersing agents in rGO composite may lead to undesirable poor performance to rGO for many technological applications.[14] Thus, it is eagerly expected that some kinds of proper molecules, introduced onto the rGO surface, can not only effectively disperse rGO but also bring in new benignant or enhanced functions for rGO.

Calixarenes, cavity-shaped cyclic phenol molecules, considered the third best host molecules after cyclodextrins and crown ethers, have been of potential interest because they can form stable host−guest complexes with various organic, inorganic, and biological guest molecules,[21−30] which show high molecular selectivity and the engaging supramolecular recognition ability. Specifically, the selective association of target molecules to the hydrophobic cavities of Calixarenes has been used to develop different sensors and separation matrices based on the strong recognition and enrichment function of
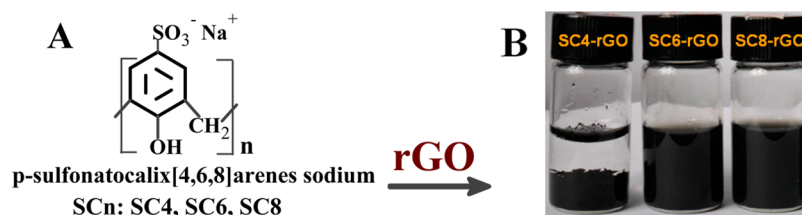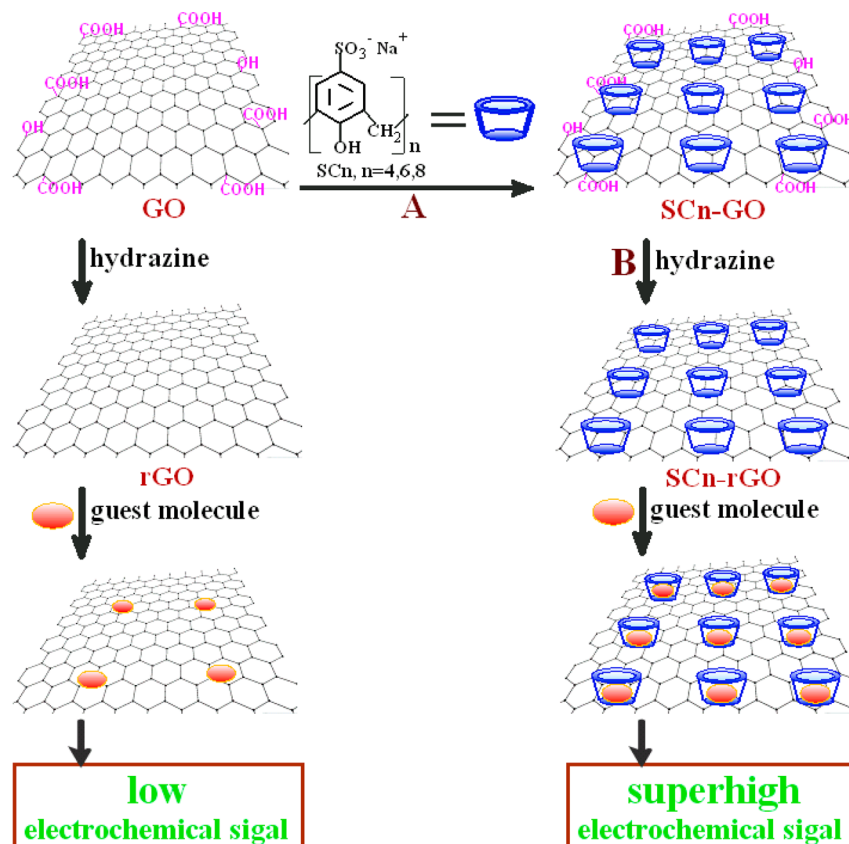
Figure 1. (A) Chemical structure of p-sulfonatocalix[4,6,8]arenes sodium [SCn: SC4, SC6, SC8]. (B) Photos of rGO in aqueous media with SC4, SC6, and SC8.

Scheme 1. Schematic Diagram of the Procedure for Preparing SCn-rGO and rGO, and Sensing the Guest Molecules by an Electrochemical Method

Calixarenes.[31−33] However, because most calixarenes have poor water-solubility, the application of calixarenes is often in organic solvents such as toluene, chloroform, dichloromethane, etc.,[34−36] which bring environmental pollution. Therefore, water-soluble calixarenes, a kind of calixarene derivative, are becoming increasingly important because of their potential use as supramolecular recognition for water-soluble dye guest molecules,[37−39] simulation enzyme models,[40] fluorescent probe in living cells,[41] catalysts,[42] and mobile phase in chromatography[43] in aqueous solution systems. Also, among water-soluble calixarenes, the most widely investigated water-soluble calixarenes are the p-sulfonated calixarene derivatives due to their benign biocompatibility and simplicity of synthesis.[41,44,45] On account of excellent performances of rGO and water-soluble calixarenes, if water-soluble calixarenes are introduced to rGO surface to form nanocomposites, through combining their individual properties, it is likely to gain new materials simultaneously possessing the large surface area and good conductivity of rGO and high supramolecular recognition and enrichment capability of calixarenes. Therefore, the integration of rGO and water-soluble calixarenes will expand potential applications in various fields such as sensors, electrocatalysis and biological probe, and thus arouse extensive research interest. So far, a few such reports appear.[46,47]

In this paper, we report on the preparation of aqueous suspension of rGO by using calixarenes through a simple wet-chemical strategy. Water-soluble p-sulfonatocalix[4,6,8]arenes sodium [SCn: SC4, SC6, SC8] were used as dispersants of rGO (Figure 1). Interestingly, rGO was dispersive in aqueous media in the presence of SC6 and SC8, while rGO was not dispersive nearly in the presence of SC4. Fourier transform infrared spectra (FTIR), Ultraviolet−visible (UV−vis) spectroscopy, thermal gravimetric analysis (TGA), contact angle measurement, scanning electron microscope (SEM), and electrochemical impedance spectroscopy (EIS) were used to characterize the structure and composition of SCn-rGO. Various characterized data showed that rGO could load a amount of SCn molecules at different degrees, which is very important for greatly enhancing the supramolecular function of SCn-rGO because of the presence of many SCn molecules on
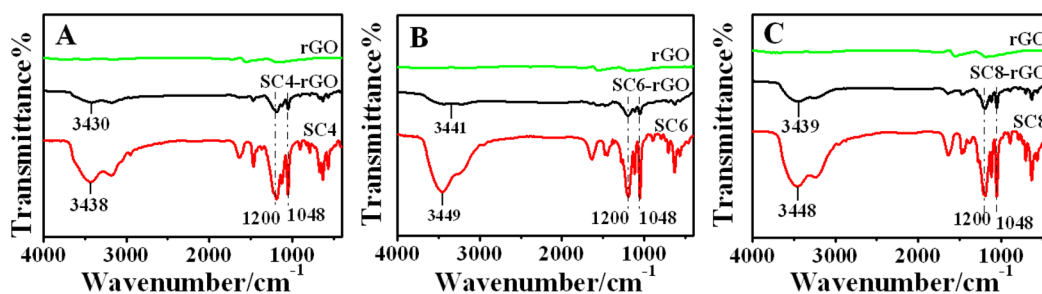
Figure 2. FT-IR spectra of (A) rGO, SC4, SC4-rGO, (B) rGO, SC6, SC6-rGO, (C) rGO, SC8, SC8-rGO.
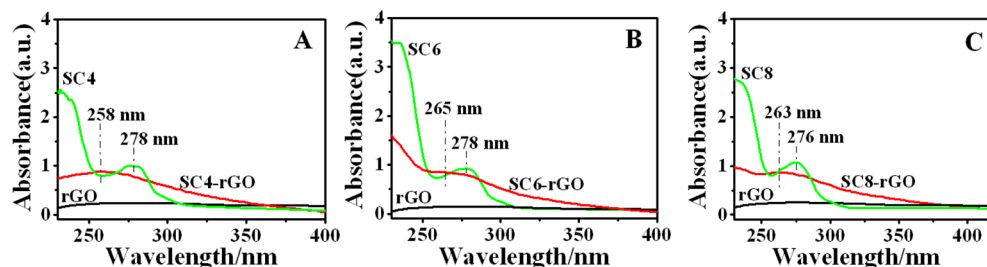

Figure 3. UV−vis spectra of (A) SC4, SC4-rGO, rGO, (B) SC6, SC6-rGO, rGO, (C) SC8, SC8-rGO, rGO.

the rGO surface. Further inspection by cyclic voltammetry measurement (CV) revealed the SCn-rGO modified glassy carbon electrode (SCn-rGO/GCE) could exhibit very high supramolecular recognition and enrichment capability and show superhigh electrochemical response to four molecules (biomolecules and dye molecules).

2. EXPERIMENTAL SECTION

2.1. Synthesis of SCn-rGO (n = 4, 6 ,8) and GO. The p-sulfonated calix[4, 6, 8]arenes sodium (SC4, SC6, SC8) were synthesized according to the literature,[48,49] and GO was synthesized from natural graphite powder by Hummer's method.[50] GO (10 mg) and SCn (20 mg) were then dispersed in deionized water (20 mL) by bath-sonicating, and the three mixtures were allowed to stir for 12 h at room temperature. After hydrazine hydrate (100 μL) and ammonia solution (200 μL) were added, the mixtures were stirred vigorously at 75 °C for 14 h. The stable black dispersion was obtained and filtered with a polycarbonate membrane (0.22 μm), and then washed with doubly distilled water three times to obtain SCn-rGO that can be readily dispersed in water (1.0 mg/mL) by ultrasonication again. In addition, the preparation of pure rGO was similar with SCn-rGO hybrid nanosheets except there was no addition of SCn.

2.2. Preparation of SCn-rGO (n = 4, 6, 8) and rGO-Modified GCE. The GCE was polished carefully with 0.3 μm-Al$_2$O$_3$ powders and then was cleaned with deionized water and sonicated in ethanol and water (each for 1 min). Then, the electrode was dried in air. a volume of 10 μL of the resulting rGO or SCn-rGO (the concentration of each carbon material was 1.0 mg/mL) was dropped onto a GCE and the electrodes were dried in air for more than 12 h. Finally, the modified electrodes were activated by several successive scans with a scan rate of 100 mV s^{-1} in 0.1 M PBS (pH 6.8).

2.3. Apparatus. UV−vis spectroscopy was measured on a UV-2550 PC UV−visible spectrometer (Shimadzu, Japan). FT-IR spectra for the various samples were recorded on a Bruker Tensor 27. SEM was applied to investigate the morphology, which was carried out with Hitachi S-4800 (Japan). Carefully weighed quantities of the different samples were subjected to TGA on a STA409PC (NETZSCH) TGA instrument at a heating rate of 10 °C·min^{-1} under vacuum from 30 to 800 °C. Contact angles were measured on a drop shape analysis system Dataphysics/OCA40 (Germany) contact angle system. EIS was measured with an Autolab/PG30 electrochemical analyzer system (ECO Chemie B. V. Netherlands) and were performed in a 0.1 M

KNO$_3$ solution containing 5 mM K$_3$[Fe(CN)$_6$] + 5 mM K$_4$[Fe(CN)$_6$] (1:1) at ambient temperature. The interfacial charge-transfer resistances for different modified surface were determined by EIS in the frequency range from 0.1 Hz to 1 MHz with a perturbation signal of 5 mV. All electrochemical experiments were carried out with a CHI660c electrochemical workstation (Chenghua, China) with a three-electrode cell including a GCE (diameter: 3 mm) as the working electrodes, a Pt wire electrode as the counter electrode and a saturated calomel electrode (SCE) as the reference electrode. All potentials reported in this paper were against SCE.

3. RESULTS AND DISCUSSION

Scheme 1 shows the procedure for preparing SCn-rGO nanocomposites and rGO, and then sensing the guest molecules by an electrochemical strategy. A typical fabrication of SCn-rGO is as follows: First, the aqueous dispersion of GO was mixed with SCn aqueous solution to form SCn-GO in ultrasonic condition (Scheme 1A). Second, the mixtures were stirred vigorously at 75 °C for 14 h after adding ammonia and hydrazine solution to prepare suspensions of SCn-rGO (Scheme 1B), and then the suspensions were filtered with a polycarbonate membrane (0.22 μm) to obtain SCn-rGO. The preparation of rGO was the same conditions as SCn-rGO except there was no addition of SCn. The chemical structures of SC4, SC6, SC8 are shown in Figure 1A. Three obtained SCn-rGO nanocomposites were dispersed in water by ultra-sonication again and the dispersive effects are shown in Figure 1B. In contrast, SC4-rGO was not dispersive nearly; SC6-rGO was not very stable, and a black precipitation appeared after two weeks, whereas SC8-rGO was extremely stable for more than two months (Figure 1B). These results indicated that the dispersity of rGO in aqueous media with water-soluble calixarenes increased in the approximate order: SC4 < SC6 < SC8. These phenomena are similar to SCn-functionalized single-walled carbon nanotubes.[51]

The synthesized SCn-rGO were characterized by Fourier transform infrared (FT-IR), by comparing FT-IR of rGO, SCn and SCn-rGO (see Figure 2), two significant features can be observed: First, the peaks for −SO$_3^-$ at 1200 and 1048 cm^{-1}, as seen in the spectra of pure SC4, SC6, and SC8, also appeared in

the spectra of SC4-rGO, SC6-rGO, and SC8-rGO, indicating that SC4, SC6, and SC8 were attached to rGO. Second, after rGO decorated by SCn, it is noted that the peak at 3438 cm^{-1} of −OH in SC4 stretching vibrations slightly shifted to 3430 cm^{-1} in SC4-rGO (see Figure 2A), similar to SC4 and SC4-rGO, the peak at 3449 cm^{-1} of −OH in SC6 stretching vibrations shifted to 3441 cm^{-1} in SC6-rGO (see Figure 2B) and the peak at 3448 cm^{-1} of −OH in SC8 stretching vibrations shifted to 3439 cm^{-1} in SC8-rGO (see Figure 2C). The O−H stretching vibration peak could exhibit typical red-shift when the hydrogen bonding is formed.[52] Here, note that the O−H stretching vibration peak for SCn-rGO exhibits slight red-shift relative to SCn. It was identified as a result of hydrogen interactions between some hydroxyl groups of SCn and some oxygen-containing groups of rGO.[41,53,54] These results illustrated that SCn had successfully self-assembled to rGO and formed SCn-rGO nanocomposites.

The successful preparation of SCn-rGO nanocomposites were confirmed by Ultraviolet−visible (UV−vis) absorption spectra. As can be seen in Figure 3, the UV−vis spectra of pure SC4, SC6 and SC8 showed a peak at 278 nm (Figure 3A), 278 nm (Figure 3B), 276 nm (Figure 3C), respectively. After SC4, SC6, and SC8 were loaded onto rGO, it is found that the absorbance peaks of SC4, SC6, and SC8 in SC4-rGO, SC6-rGO and SC8-rGO shifted to 258 nm, 265 nm, 263 nm (Figure 3A−C), which indicated that SCn had been adsorbed onto rGO. However, corresponding peaks did not observed from rGO. The result also confirmed that SCn had been successfully introduced into rGO.

TGA was used to determine the amount of SCn molecules on the surface of rGO. Figure 4 displays the weight losses of
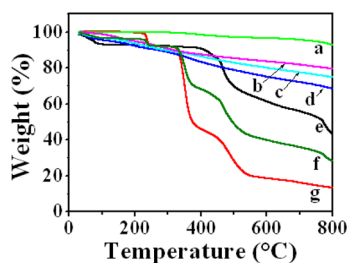

Figure 4. TGA of (a) rGO, (b) SC4-rGO, (c) SC6-rGO, (d) SC8-rGO, (e) SC4, (f) SC6, (g) SC8.

rGO (curve a), SC4-rGO (curve b), SC6-rGO (curve c), SC8-rGO (curve d), SC4 (curve e), SC6 (curve f), SC8 (curve g). Pure SC4, SC6 and SC8 slowly decomposed at approximately 400 °C, 350 and 330 °C, respectively. rGO showed much higher thermal stability with only a mass loss of 5.8% up to 800 °C. As to the nanocomposite SC4-rGO, SC6-rGO and SC8-rGO, deducted mass loss of rGO, the weight losses were attributed to the decomposition of SC4, SC6, SC8 were 14.2, 18.2, and 26.4%, respectively, indicating that the amount of

SCn molecules functionalized on the surface of rGO increased with the increase of the value of n in SCn ($n = 4, 6, 8$). That to say, the amount of SCn molecules covered on the surface of rGO in the order was SC8-rGO > SC6-rGO > SC4-rGO. This is an exciting result because rGO loading plentiful SCn molecules will have a good opportunity to expand the supramolecular recognition and enrichment ability of SCn.

SCn-rGO were further characterized with the static contact angle measurement to investigate their hydrophilic/hydrophobic features. The contact angles for water of rGO, SC4-rGO, SC6-rGO and SC8-rGO film were measured to be 77, 57, 40, and 26°, respectively (Figure 5A−D). It is noted that the unmodified rGO had a relatively hydrophobic interface and the interfaces of SCn-rGO were comparatively more hydrophilic, which indicate that the rGO was modified by water-soluble SCn molecules. And also, it is easily seen that the contact angles of SC4-rGO, SC6-rGO, and SC8-rGO film gradually became smaller. The comparison of the contact angle of SCn-rGO revealed that the hydrophilicity of SCn-rGO gradually increased from SC4-rGO, SC6-rGO to SC8-rGO. Consequently, it could be deduced that the amount of water-soluble SCn molecules decorated onto the rGO should be in the order SC8 > SC6 > SC4.

To investigate the degree of dispersion of rGO, SC4-rGO, SC6-rGO, and SC8-rGO in aqueous media, we applied scanning electron microscopy (SEM) to research the surface topography of rGO, SC4-rGO, SC6-rGO, and SC8-rGO after they were dripped to substrate and dried. As for unmodified rGO, as shown in Figure 6A, B, larger particles were seen clearly because of rGO aggregation. After rGO was modified by SCn, particles of SCn-rGO disappeared gradually and homogeneous films formed by degree from SC4-rGO (Figure 6C, D), SC6-rGO (Figure 6E, F) and SC8-rGO (Figure 6G, H) because of the introduction of hydrophilic SCn molecules across the rGO basal plane. Especially, SC8-rGO could form a smooth, homogeneous and wrinkled film structure on the substrate. This change suggested that the dispersive capacity of SC4, SC6, and SC8 for rGO was increasing with the increase of the number of phenolic units in the calixarene ring in aqueous solution. These important characteristics enable SCn-rGO to be a good material for electrochemical sensors.

EIS is a useful way for probing the characters of a surface-modified electrode material for an ultracapacitor. The semi-circle portion observed at high frequencies in Nyquist diagrams corresponds to the charge transfer limiting process,[55] and the charge transfer resistance (R_{ct}) values can be directly measured as the diameter of the semicircle. Figure 7 displays the results of impedance spectroscopy on bare GCE (curve a), rGO/GCE (curve b), SC4-rGO/GCE (curve c), SC6-rGO/GCE (curve d) and SC8-rGO/GCE (curve e) in the presence of equivalent 5.0 mM Fe(CN)$_6^{3-/4-}$. The R_{ct} of bare GCE (254 Ω) was largest, indicating that the polarization resistance of bare GCE was the biggest one among the five electrodes. When rGO was modified

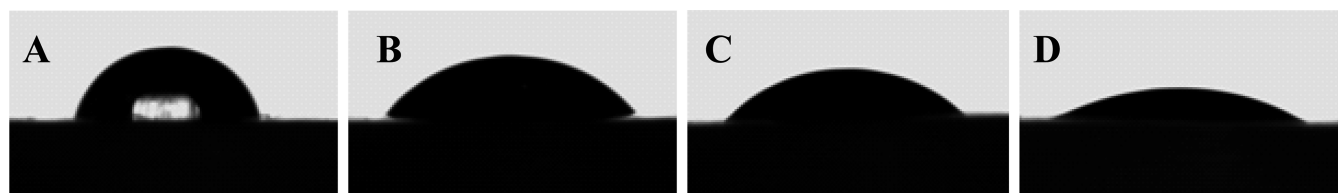**Figure 5.** Shape of a water droplet on the surface of (A) rGO, (B) SC4-rGO, (C) SC6-rGO, (D) SC8-rGO.
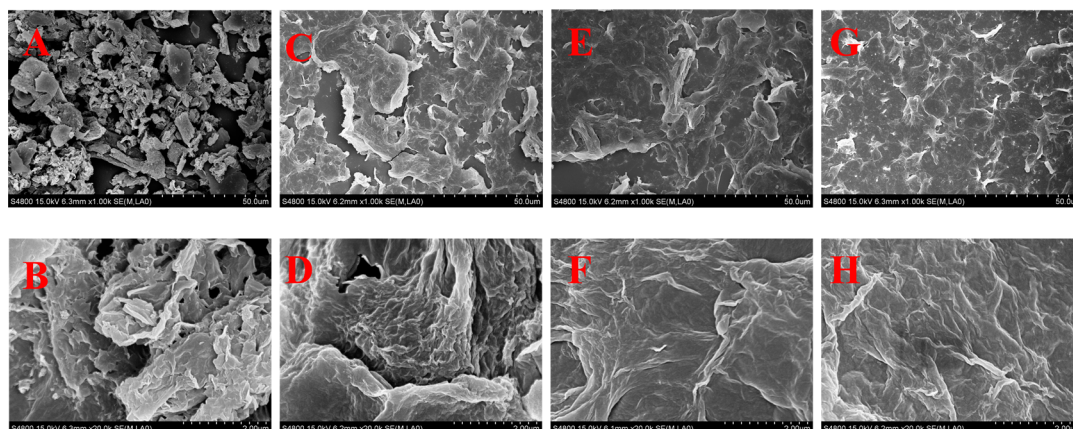
Figure 6. SEM images of (A, B) rGO, (C, D) SC4-rGO, (E, F) SC6-rGO, (G, H) SC8-rGO on the substrate at different magnifications.
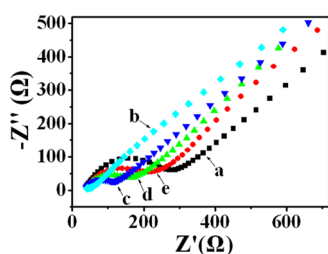

Figure 7. Nyquist plots for (a) bare GCE, (b) rGO/GCE, (c) SC4-rGO/GCE, (d) SC6-rGO/GCE, (e) SC8-rGO/GCE in 0.1 M KNO$_3$ solution containing 5.0 mM Fe(CN)$_6^{3-/4-}$.

on the surface of the GCE, the R_{ct} value decreased dramatically, which was due to the excellent electronic property of rGO that formed a fast electron conduction pathway between the electrode and the electrochemical probe Fe(CN)$_6^{3-/4-}$. For SC4-rGO, SC6-rGO and SC8-rGO, R_{ct} values were 88, 123, and 202 Ω, respectively, and any one of three R_{ct} values was larger than rGO. This was mainly attributed to nonconducting SCn molecules loaded on rGO lead to the increase of the resistance of rGO. Furthermore, the R_{ct} values of SCn-rGO gradually increased from SC4-rGO, SC6-rGO to SC8-rGO, indicating the amount of SCn molecules introduced onto the surface of rGO increased with the increase of the value of n in SCn (n = 4, 6, 8). The result is consistent with other characterization, such as TGA and the contact angle.

Considering the molecular structure of rGO and SCn, the self-assembly mechanism of SCn on the surface of rGO is mainly attributed to π−π interactions and hydrogen interactions. On the one hand, the noncovalent functionalization of rGO through π−π interactions using aromatic organic molecules has been addressed in some literatures.[56−58] Here, hydrophobic segments of benzene rings of SCn may be adsorbed to the rGO surface by π−π interactions. As is well-known, increasing the macrocycle size of calixarenes usually brings about an increase in conformational flexibility.[59,60] Obviously, because of the most flexible conformation of SC8, the hydrophobic segments of the benzene ring of SC8 may be the most easily adsorbed to the rGO surface compared to that of SC4 and SC6. In the same way, SC6 is more easily modified to the rGO surface than SC4. On the other hand, it was verified that there were hydrogen interactions between some oxygen-containing groups of rGO and hydroxyl groups of p-sulfonated calixarenes,[41] which was strongly confirmed by our FT-IR spectra. The number of hydroxyl groups of p-sulfonated

calixarenes increases with the increase of the value of n in SCn (n = 4, 6, 8), resulting in the enhanced interaction between rGO and SCn from SC4 and SC6 to SC8. Therefore, through two driving forces, the behaviors of SCn molecules self-assembly on the surface of rGO become easy. At the same time, with the increase of the number of phenolic units in the calixarene ring, it is accompanied by the driving force increase in the order of SC4-rGO < SC6-rGO < SC8-rGO. Meanwhile, the hydrophilic parts of SCn prevent rGO from aggregating in aqueous solution. As a result, the water-dispersity of SCn-rGO is SC4-rGO < SC6-rGO < SC8-rGO.

On the basis of the above discussion, all kinds of characterization methods demonstrated that a number of SCn moleculars had been loaded onto the surface of rGO, which could not only improve the dispersion and stability of rGO at different degrees but also be expected to apply to improve the sensitivity of detection for some biological molecules and organic dye molecules through the formation of supramolecular complexes between SCn and the guest molecules that fit spatially within the cavities of SCn. To verify this conceive (Scheme 1), the electrochemical behaviors were investigated for four kinds of electroactive molecules [dopamine (DA), uric acid (UA), tryptophan (Trp), methylene blue (MB)] that can form inclusion complexes with SCn. Cyclic voltammograms (CVs) and peak current of CVs of 50 μM DA at GCE (a), rGO/GCE (b), SC4-rGO/GCE (c), SC6-rGO/GCE (d) and SC8-rGO/GCE (e) are shown in A and B in Figure 8, respectively. In curve a, there were very weak redox peaks on the bare GCE. However, in curve b, the oxidation peak currents of DA increased at rGO/GCE relative to that at the bare GCE, which may be attributed to superior conductivity and large surface area of rGO resulting from its unique structure. To our excitement, at the SCn-rGO/GCE (from curve c−e), all showed a very remarkable increase in the peak currents relative to that at the bare GCE and rGO/GCE. In Figure 8B, the peak current at SC4-rGO/GCE was about 80 times as much as that at bare GCE and approximately 4 times as much as that at rGO/GCE. The peak current at SC6-rGO/GCE was about 100 times as much as that at bare GCE and approximately 5 times as much as that at rGO/GCE. It is extremely surprised that at SC8-rGO/GCE the peak current was more than 150 times as much as that at the bare GCE and about 10 times as much as that at rGO/GCE, as can be seen in Figure 8B. According to the result of the experiment, SC8/GCE, SC6/GCE, and SC4/GCE showed the high current densities of 73.04, 42.19, and
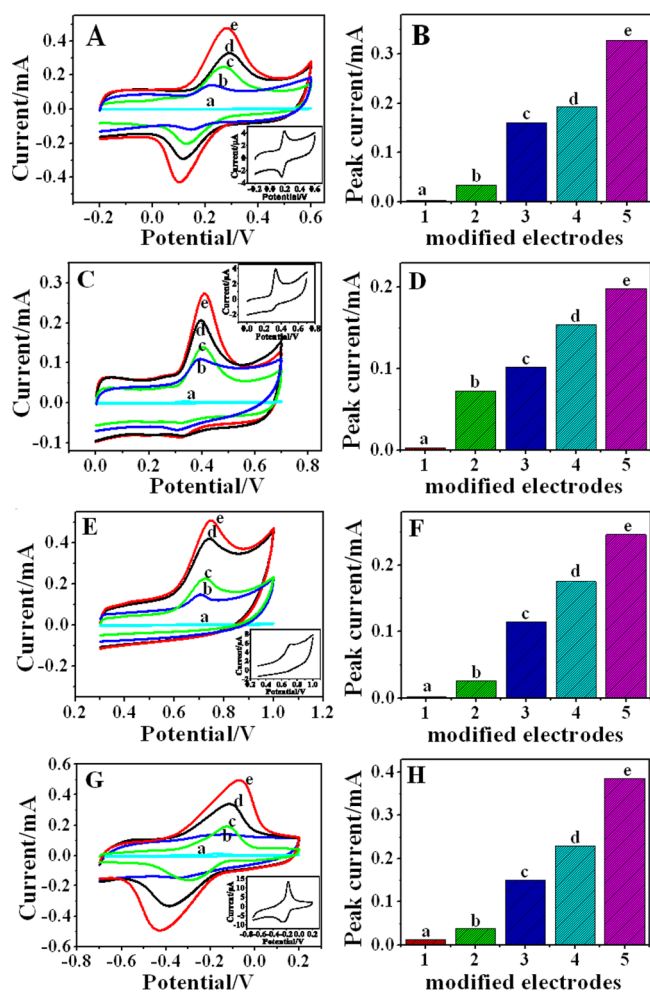
Figure 8. CVs and peak current of CVs of (A, B) 50 μM DA, (C, D) UA, (E, F) Trp, (G, H) MB at (a) bare GCE, (b) rGO/GCE, (c) SC4-rGO/GCE, (d) SC6-rGO/GCE, and (e) SC8-rGO/GCE in 0.1 M phosphate buffer (pH 6.8). Inset: CVs of (A) 50 μM DA, (C) UA, (E) Trp, (G) MB at bare GCE in 0.1 M phosphate buffer (pH 6.8).

36.51 mA mM^{-1} L cm^{-2} for DA, respectively. So far as we know, any of them are much higher than those of recently reported nanomaterials, such as CNTs/quercetin/Nafion composite film (about 0.122 mA mM^{-1} L cm^{-2}),[61] graphene (0.278 mA mM^{-1} L cm^{-2}),[62] CD-graphene (6.93 mA mM^{-1} L cm^{-2}),[47] respectively. The similar results have also been obtained to UA (Figure 8C, D), Trp (Figure 8E, F) and MB (Figure 8G, H).

According to above experiential results, SCn molecules on the surface of rGO with superhigh supramolecular recognition capability could not only prevent the aggregation of rGO and meanwhile increase the effective area, but also form host–guest complexes with all the investigated analytes. The interaction between the guest and the host could further enhance the accumulation effect of SCn-rGO/GCE and accordingly increase the concentration of analytes on the interface of the modified electrode, which resulted in the noteworthy enlargement of the peak current. These phenomena indicated that SCn-rGO not only exhibited the prominent properties of rGO but also displayed the outstanding supramolecular recognition capability of SCn. Therefore, the immobilized SCn moleculars on the rGO surface greatly enhanced electrochemical performance and

simultaneously improved the sensitivity of detection for target molecules.

As introduced above, the enrichment effect of SCn-rGO was very prominent and improved the electrochemical reactivity for analytes. Obviously, there were distinctively different enrichment effect among SC4-rGO, SC6-rGO, and SC8-rGO. On the basis of the peak current response of CVs for analytes, it is easily seen that enrichment effect of SC4-rGO, SC6-rGO, and SC8-rGO in the order was SC8-rGO > SC6-rGO > SC4-rGO. This result can be expounded from the following: First of all, the cavity size of SCn may affect the enrichment effect of SCn-rGO for target molecules. Some efforts have proved that the inclusion ability of SCn increase with the increase of the value of n in SCn (n = 4, 6, 8).[32,39] Our experimental results showed the larger the cavity size of the host SC8-rGO accommodated the larger capacity of gust molecules than that of SC6-rGO or SC4-rGO, which is consistent with reports. Second, the enrichment effects of modified electrodes may depend on the loading amount of SCn molecules on the rGO surface. The more SCn molecules can provide the more opportunity for developing their supramolecular recognition and enrichment functions. The loading amount of SCn molecules on the rGO surface increased in the order of SC4-rGO, SC6-rGO, and SC8-rGO confirmed by TGA, contact angle and EIS, which resulted in the enhancement of the enrichment effect of SCn-rGO for target molecules from SC4-rGO, SC6-rGO to SC8-rGO. Last, with the increase of the value of n in SCn (n = 4, 6, 8), the film of SCn-rGO on the substrate became more homogeneous from SC4-rGO, SC6-rGO to SC8-rGO, which was demonstrated by SEM. The varying trend could enhance the effective surface area of rGO and accordingly lead to the enhancement of peak current in varied degrees from SC4-rGO, SC6-rGO to SC8-rGO.[47]

It was reported that SC4, SC6, SC8 could be oxidized and the anodic peak potential was in the potential region about 0.7–1.0 V.[63−65] Therefore, it was investigated that the electrochemical reaction of SC4-rGO, SC6-rGO, and SC8-rGO modified on the GCE in the blank phosphate buffer solution (PBS) in corresponding experimental potential window for DA (see Figure S1 in the Supporting Information), UA (see Figure S2 in the Supporting Information), Trp (see Figure S3 in the Supporting Information) and MB (see Figure S4 in the Supporting Information) to see if there was the interference anodic peak of SCn. As for DA, Figure S1 in the Supporting Information shows CVs of 0.1 M blank PBS (curve a) and 50 μM DA in 0.1 M PBS (curve b) at SC4-rGO/GCE (see Figure S1A in the Supporting Information), SC6-rGO/GCE (see Figure S1B in the Supporting Information) and SC8-rGO/GCE (see Figure S1C in the Supporting Information), respectively. It can be seen that no electrochemical reaction of SC4, SC6, SC8 occurred in the −0.2−0.6 V in 0.1 M blank PBS. However, there were high redox peak current of DA when 50 μM DA was present in the PBS. The result indicated SC4, SC6, SC8 did not affect the value of peak current of DA. Obviously, the similar results have also been obtained from UA, Trp, and MB.

According to the above discussion, among SC8-rGO, SC6-rGO, and SC4-rGO, apparently, SC8-rGO was the best electrode material for improving the electrochemical reactivity for analytes. To demonstrate the sensing performance of SCn-rGO toward certain substance, we chosen SC8-rGO as the represent of electrode material and DA (its concentration detection is important for the early diagnosis of many

neurological illnesses) was chosen as a representative analyte. Then, SC8-rGO was used to modify GCE to detect DA electrochemically using the differential pulse voltammetry (DPV). Figure 9A shows DPV response for different
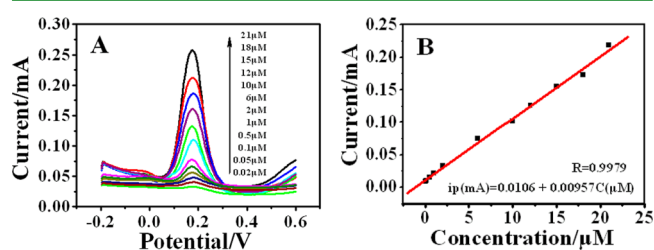

Figure 9. (A) DPV response for the different concentrations of DA at SC8-rGO/GCE in 0.1 M PBS (pH 6.8). (B) The calibration curve of DA.

concentrations of DA. A clearly defined oxidation current versus the concentration of DA had a good linearity in the range from 1×10^{-8} to 2.1×10^{-5} mol L^{-1} (Figure 9B). The regression equation was i (mA) = 0.0106 + 0.00957 C_{DA} (μM) with a correlation coefficient of R = 0.9979, and the detection limit was evaluated to be 8×10^{-9} mol L^{-1} based on 3 signal−noise ratio. This analytical performance can be compared with those of recent state-of-art carbon nanomaterial in the literature for the table 1. It is very obvious that the detection limit and

Table 1. Comparison Analytical Performance of Some Modified Electrodes for the Determination of DA

modified electrodes	linear range/ DPV	detection limit	ref
single-walled carbon nanohorn/GCE	0.2−3.8 μM	0.06 μM	66
mesoporous carbon nanofiber/ pyrolytic graphite electrode	0.05−30 μM	0.02 μM	67
carbon-nanofiber/carbon-paste electrode	0.04−5.6 μM	0.04 μM	68
Pt nanoparticles decorated the multiwall carbon nanotube/GCE	0.043−62 μM	0.028 μM	69
graphene/GCE	5−200 μM		70
Pt/graphene nanocomposite/GCE	0.03−8.13 μM	0.03 μM	71
chitosan−graphene/GCE	1.0−24 mM	1.0 mM	72
β-CD−multiwall carbon nanotubes/ GCE	0.01−0.08 mM	37 μM	73
CD−graphene/GCE	0.1−18 μM	20 nM	47
calixarene−graphene/GCE	0.01−21 μM	8 nM	this work

linear range obtained by SC8-rGO modified electrode is preferable. These comparison data indicate that the SC8-rGO/GCE exhibited very high electrochemical performance toward the target molecules. Therefore, based on an electrochemical technique, SCn-rGO can be applied to the development of sensitive electrochemical sensors to determine a wide variety of electroactive compounds.

To investigate the selectivity to the substrates at SC8-rGO/GCE, we chosen DA as a representative analyte and ascorbic acid (AA), UA, Trp were used as the interfering substance. Figure 10A shows CVs of 50 μM AA (black curve) in 0.1 M PBS at SC8-rGO/GCE. Interestingly, it is found that no electrochemical reaction occurred in 0.1 M PBS containing 50 μM AA at SC8-rGO/GCE, indicating AA do not interfere with the determination of DA. In Figure 10A, red curve shows CVs
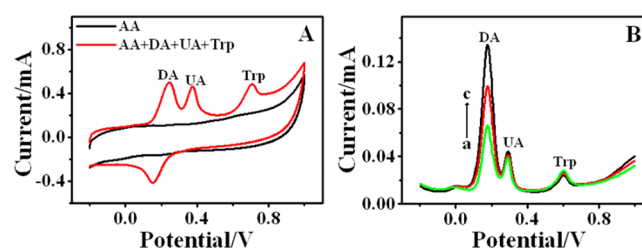

Figure 10. (A) CVs of 50 μM AA 0.1 M PBS (pH 6.8) (black curve) and 50 μM DA + 50 μM UA + 50 μM Trp +50 μM AA in 0.1 M PBS (pH 6.8) at SC8-rGO/GCE (red curve). (B) DPV curves of 50 μM UA and 50 μM Trp with different concentration of DA: (a → c) 5, 10, 15 μM in 0.1 M PBS (pH 6.8) at SC8-rGO/GCE.

of 50 μM DA + 50 μM UA + 50 μM Trp +50 μM AA in 0.1 M PBS at SC8-rGO/GCE. There are three independent anodic peaks corresponding to DA (0.24 V), UA (0.38 V), and Trp (0.70 V), respectively, which shows that under the experimental conditions, three electroactive compounds have no interference by each other and may be detected simultaneously. Furthermore, we detected different concentrations of DA by using DPV at SC8-rGO/GCE when UA and Trp were present in electrolytic cell. In Figure 10B, it is similar to the result of CV. Three separated anodic peaks are attributed to DA, UA and Trp, respectively. When concentrations of DA increase from 5, 10, to 15 μM (curve a → c), the currents versus the concentration of DA increase linearly. On the other hand, the anodic peaks of UA and Trp have no change. The result shows that UA and Trp do not interfere with the determination of DA, which indicates that the SC8-rGO/GCE has relatively good selectivity for DA.

In general, the complex interaction is attributed to the weak forces including hydrogen bonding, hydrophobic interaction, π−π interactions, electrostatic interaction, and dipole−dipole interactions. Additionally, the geometrical shape, size of the guest, and the cavity size of the host are important factors in forming host−guest inclusion complexes.

In our study, the calixarenesulfonates-rGO/GCE showed high analytical performance for the determination of DA compared with other examples. This result can be expounded from the interactions between calixarenesulfonates and DA, i.e., electrostatic interaction, hydrogen bonding and hydrophobic interaction. To discuss the problem, we chosen SC8-rGO as the represent of electrode material. As for electrostatic interaction, because SC8 has a negative charge and DA has a positive charge, there is an intense electrostatic attraction between SC8 and DA (see Figure S5 in the Supporting Information: at the upper rim of SC8), which results into the strong interactions between SC8 and DA. However, UA and Trp carry with negative charge, so the similar result cannot be obtained. Moreover, because a molecule of DA has two hydroxyl groups and one amino group that can form hydrogen bonding with hydroxyl groups of SC8, there should be stronger hydrogen bonding between SC8 and DA compared with other examples (see Figure S5 in the Supporting Information: at the lower rim of SC8). At last, hydrophobic interaction is attributed to the influence of size effect. SC8 has a cavity of 7 Å depth and diameter of 11.7 Å,[74] as shown in Figure S6 in the Supporting Information. One dimension size of DA molecule is 4.5 Å and smaller than other examples (UA, 5.1 Å; Trp, 5.5 Å; MB,5.2 Å), as shown in Figure S7 in the Supporting Information. So it is easiest to enter the cavity of SC8 for DA molecules that can

834

dx.doi.org/10.1021/am302289v | *ACS Appl. Mater. Interfaces* 2013, 5, 828−836

increase the analytical performance (see Figure S5 in the Supporting Information: in the cavity of SC8). In conclusion, the synergy of three forces can enhance interactions and lead to highest association constant between SC8 and DA (see Table S1 in the Supporting Information), so the calixarenesulfonates-rGO/GCE showed higher analytical performance for the determination of DA compared with other examples.

4. CONCLUSION

In conclusion, we have developed a facile and rapid method for the synthesis of SCn-rGO (n = 4, 6, 8) hybrid nanosheets, which exhibited the increase of water-dispersity and stability from SC4-rGO, SC6-rGO to SC8-rGO. More significantly, three kinds of new hybrid composites SCn-rGO (n = 4, 6, 8) modified GCE all exhibited outstanding supramolecular recognition and much higher electrochemical response to four target molecules than those of rGO/GCE and bare electrodes. Furthermore, the size of CV current for the same target molecule in the order was SC8-rGO > SC6-rGO > SC4-rGO in the same conditions, which indicated that the SCn-rGO not only showed the good electrical and high-surface-area properties of rGO but also exhibited high supramolecular recognition and enrichment properties of SCn. The result revealed three SCn-rGO composites would probably develop wide applications in various fields because of the tunable cavity size of different kinds of SCn.

ASSOCIATED CONTENT

Ⓢ Supporting Information

CVs of 0.1 M blank PBS and 50 μM DA, UA, Trp, and MB in 0.1 M PBS at different modified electrodes, the association constants between substrates and SC8, Schematic Diagram of the interaction between SC8 and DA, molecular models of DA, UA, Trp, MB, and Calculated Molecular dimensions. This information is available free of charge via the Internet at http://pubs.acs.org.

AUTHOR INFORMATION

Corresponding Author
*E-mail: gwdiao@yzu.edu.cn.

Notes
The authors declare no competing financial interest.

ACKNOWLEDGMENTS

REFERENCES

(1) Lee, C.; Wei, X. D.; Kysar, J. W.; Hone, J. *Science* **2008**, *321*, 385−388.

(2) Stoller, M. D.; Park, S. J.; Zhu, Y. W.; An, J. H.; Ruoff, R. S. *Nano Lett.* **2008**, *8*, 3498−3502.

(3) Service, R. F. *Science* **2008**, *322*, 1785−1785.

(4) Xu, C.; Wang, X.; Zhu, J. W. *J. Phys. Chem. C* **2008**, *112*, 19841−19845.

(5) Yoo, E. J.; Okata, T.; Akita, T.; Kohyama, M.; Nakamura, J.; Honma, I. *Nano Lett.* **2009**, *9*, 2255−2259.

(6) Zhu, C.; Guo, S.; Zhai, Y.; Dong, S. *Langmuir* **2010**, *26*, 7614−7618.

(7) Lu, J.; Do, I.; Drzal, L. T.; Worden, R. M.; Lee, I. *ACS Nano* **2008**, *2*, 1825−1832.

(8) Guo, S.; Wen, D.; Zhai, Y.; Dong, S.; Wang, E. *ACS Nano* **2010**, *4*, 3959−3968.

(9) Si, Y.; Samulski, E. *Chem. Mater.* **2008**, *20*, 6792−6797.

(10) Li, Y.; Lv, X.; Lu, J.; Li, J. *J. Phys. Chem. C* **2010**, *114*, 21770−21774.

(11) Li, X. L.; Wang, X. R.; Zhang, L.; Lee, S.; Dai, H. J. *Science* **2008**, *319*, 1229−1232.

(12) Di, C.- A.; Wei, D. C.; Yu, G.; Liu, Y. Q.; Guo, Y. L.; Zhu, D. B. *Adv. Mater.* **2008**, *20*, 3289−3293.

(13) Xu, Y.; Liu, Z.; Zhang, X.; Wang, Y.; Tian, J.; Huang, Y.; Ma, Y.; Zhang, X.; Chen, Y. *Adv. Mater.* **2009**, *21*, 1275−1279.

(14) Si, Y.; Samulski, E. T. *Nano Lett.* **2008**, *8*, 1679−1682.

(15) Xu, Y.; Wang, Y.; Liang, J.; Huang, Y.; Ma, Y.; Wan, X.; Chen, Y. *Nano Res.* **2009**, *2*, 343−348.

(16) Xu, Y.; Bai, H.; Lu, G.; Li, C.; Shi, G. *J. Am. Chem. Soc.* **2008**, *130*, 5856−5857.

(17) Liu, H.; Gao, J.; Xue, M.; Zhu, N.; Zhang, M.; Cao, T. *Langmuir* **2009**, *25*, 12006−12010.

(18) Liu, F.; Choi, J. Y.; Seo, T. S. *Chem. Commun.* **2010**, *46*, 2844−2846.

(19) Patil, A. J.; Vickery, J. L.; Scott, T. B.; Mann, S. *Adv. Mater.* **2009**, *21*, 3159−3164.

(20) Stankovich, S.; Piner, R. D.; Chen, X.; Wu, N.; Nguyen, S. T.; Ruoff, R. S. *J. Mater. Chem.* **2006**, *16*, 155−158.

(21) Diamond, D.; McKervey, M. A. *Chem. Soc. Rev.* **1996**, *25*, 15−24.

(22) Steed, J. W. *Science* **2002**, *298*, 976−977.

(23) Troisi, F.; Russo, A.; Gaeta, C.; Bifulco, G.; Neri, P. *Tetrahedron Lett.* **2007**, *48*, 7986−7989.

(24) Bonaccorso, C.; Sgarlata, C.; Grasso, G.; Zito, V.; Sciotto, D.; Arena, G. *Chem. Commun.* **2011**, *47*, 6117−6119.

(25) Hamdi, A.; Kim, S. H.; Abidi, R.; Thuéry, P.; Kim, J. S.; Vicens, J. *Tetrahedron* **2009**, *65*, 2818−2823.

(26) Zorzi, R. D.; Guidolin, N.; Randaccio, L.; Purrello, R.; Geremia, S. *J. Am. Chem. Soc.* **2009**, *131*, 2487−2489.

(27) Lopez-Cornejo, P.; Bote, B.; Felix, R.; Infantes, I.; Lopez, P.; Martin, A.; Mateos, E.; Perez, M.; Rojas, A.; Suarez, R. *J. Phys. Chem. B.* **2009**, *113*, 12721−12726.

(28) Notestein, J. M.; Solovyov, A.; Andrini, L. R.; Requejo, F. G.; Katz, A.; Iglesia, E. *J. Am. Chem. Soc.* **2007**, *129*, 15585−15595.

(29) Pacioni, N. L.; Occello, V. N. S.; Lazzarotto, M.; Veglia, A. V. *Anal. Chim. Acta* **2008**, *624*, 133−140.

(30) Tu, C.; Zhu, L.; Li, P.; Chen, Y.; Su, Y.; Yan, D.; Zhu, X.; Zhou, G. *Chem. Commun.* **2011**, *47*, 6063−6065.

(31) Carrillo-Carrión, C.; Lendl, B.; Simonet, B. M.; Valcárcel, M. *Anal. Chem.* **2011**, *83*, 8093−8100.

(32) Chen, M.; Chen, Y.; Diao, G. *J. Chem. Eng. Data* **2010**, *55*, 5109−5116.

(33) Sayin, S.; Yilmaz, M.; Tavasli, M. *Tetrahedron.* **2011**, *67*, 3743−3753.

(34) Tripp, S. L.; Pusztay, S. V.; Ribbe, A. E.; Wei, A. *J. Am. Chem. Soc.* **2002**, *124*, 7914−7915.

(35) Ciesa, F.; Plech, A.; Mattioli, C.; Pescatori, L.; Arduini, A.; Pochini, A.; Rossi, F.; Secchi, A. *J. Phys. Chem. C* **2010**, *114*, 13601−13607.

(36) Ha, J.-M.; Solovyov, Andrew.; Katz, A. *Langmuir* **2009**, *25*, 10548−10553.

(37) Liu, Y.; Han, B. H.; Chen, Y. T. *J. Org. Chem.* **2000**, *65*, 6227−6230.

(38) Liu, Y.; Han, B.-H.; Chen, Y.-T. *J. Phys. Chem. B.* **2002**, *106*, 4678−4687.

(39) Chen, M.; Diao, G. W. *J. Solution Chem.* **2011**, *40*, 481−491.

(40) Rondelez, Y.; Rager, M. N.; Duprat, A.; Reinaud, O. *J. Am. Chem. Soc.* **2002**, *124*, 1334−1340.

(41) Mao, X.; Tian, D.; Li, H. *Chem. Commun.* **2012**, *48*, 4851−4853.

(42) Karakhanov, E.; Buchneva, T.; Maximov, A.; Zavertyaeva, M. *J. Mol. Catal. A−Chem.* **2002**, *184*, 11−14.

(43) Liu, M.; Li, L. S.; Da, S. L.; Feng, Y. Q. *Talanta* **2005**, *66*, 479−486.

(44) Douteau-Guével, N.; Coleman, A. W.; Morel, J.-P.; Morel-Desrosiers, N. *J. Phys. Org. Chem.* **1998**, *11*, 693−696.

(45) Specht, A.; Ziarelli, F.; Bernard, P.; Goeldner, M.; Peng, L. *HeIv. Chim. Acta.* **2005**, *88*, 2641−2653.

(46) Konkena, B.; Vasudevan, S. *Langmuir* **2012**, *28*, 12432−12437.

(47) Guo, Y.; Guo, S.; Ren, J.; Zhai, Y.; Dong, S.; Wang, E. *ACS Nano* **2010**, *4*, 4001−4010.

(48) Shinkai, S.; Araki, K.; Tsubaki, T.; Arimura, T.; Manabe, O. *J. Chem. Soc., Perkin Trans. 1* **1987**, 2297−2299.

(49) Shinkai, S.; Mori, S.; Koreishi, H.; Tsubaki, T.; Manabe, O. *J. Am. Chem. Soc.* **1986**, *108*, 2409−2416.

(50) Hummers, W. S.; Offeman, R. E. *J. Am. Chem. Soc.* **1958**, *80*, 1339−1339.

(51) Ogoshi, T.; Yamagishi, T.; Nakamoto, Y. *Chem. Commun.* **2007**, 4776−4778.

(52) Scatena, L. F.; Brown, M. G.; Richmond, G. L. *Science* **2001**, *292*, 908−912.

(53) Park, S.; Ruoff, R. S. *Nat. Nanotechnol.* **2009**, *4*, 217−224.

(54) Dreyer, D. R.; Park, S.; Bielawski, C. W.; Ruoff, R. S. *Chem. Soc. Rev* **2010**, *39*, 228−240.

(55) Guo, H. L.; Wang, X. F.; Qian, Q. Y.; Wang, F. B.; Xia, X. H. *ACS Nano* **2009**, *3*, 2653−2659.

(56) Yang, X.; Xu, M.; Qiu, W.; Chen, X.; Deng, M.; Zhang, J.; Iwai, H.; Watanabe, E.; Chen, H. *J. Mater. Chem.* **2011**, *21*, 8096−8103.

(57) Xu, Y.; Bai, H.; Lu, G.; Li, C.; Shi, G. *J. Am. Chem. Soc.* **2008**, *130*, 5856−5857.

(58) Liu, H.; Gao, J.; Xue, M.; Zhu, N.; Zhang, M.; Cao, T. *Langmuir* **2009**, *25*, 12006−12010.

(59) Yamagishi, T.; Moriyama, E.; Konishi, G.; Nakamoto, Y. *Macromolecules* **2005**, *38*, 6871−6875.

(60) Atwood, J. L.; Dalgarno, S. J.; Hardie, M. J.; Raston, C. L. *Chem. Commun.* **2005**, 337−339.

(61) Chen, P.-Y.; Vittal, R.; Nien, P.-C.; Ho, K.-C. *Biosens. Bioelectron.* **2009**, *24*, 3504−3509.

(62) Zhou, M.; Zhai, Y. M.; Dong, S. J. *Anal. Chem.* **2009**, *81*, 5603−5613.

(63) Diao, G.; Zhou, Wei. *J. Electroanal. Chem.* **2004**, *567*, 325−330.

(64) Diao, G.; Liu, Y. *Electroanalysis* **2005**, *17*, 1279−1284.

(65) Chen, M.; Wang, H. L.; Gu, J.; Diao, G. W. *J. Appl. Electrochem.* **2007**, *37*, 331−337.

(66) Zhu, S.; Li, H.; Niu, W.; Xu, G. *Biosens. Bioelectron.* **2009**, *25*, 940−943.

(67) Yue, Y.; Hu, G.; Zheng, M.; Guo, Y.; Cao, J.; Shao, S. *Carbon* **2012**, *50*, 107−114.

(68) Liu, Y.; Huang, J.; Hou, H.; You, T. *Electrochem. Commun.* **2008**, *10*, 1431−1434.

(69) Dursun, Z.; Gelmez, B. *Electroanalysis* **2010**, *22*, 1106−1114.

(70) Wang, Y.; Li, Y.; Tang, L.; Lu, J.; Li, J. *Electrochem. Commun.* **2009**, *11*, 889−892.

(71) Sun, C. L.; Lee, H. H.; Yang, J. M.; Wu, C. C. *Biosens. Bioelectron.* **2011**, *26*, 3450−3455.

(72) Han, D.; Han, T.; Shan, C.; Ivaska, A.; Niu, L. *Electroanalysis* **2010**, *22*, 2001−2008.

(73) Alarcon-Angeles, G.; Perez-Lopez, B.; Palomar-Pardave, M.; Ramirez-Silva, M. T.; Alegret, S.; Merkoci, A. *Carbon* **2008**, *46*, 898−906.

(74) Kaliappan, R.; Ling, Y.; Kaifer, A. E.; Ramamurthy, V. *Langmuir* **2009**, *25*, 8982−8992.

836

dx.doi.org/10.1021/am302289v | *ACS Appl. Mater. Interfaces* 2013, 5, 828−836